JOURNAL OF OPTOELECTRONICS AND ADVANCED MATERIALS, Vol. 11, No. 9, September 2009, p. 1072 - 1078

Characterisation and optimisation of amorphous silicon / crystalline silicon heterojunction solar cells

R. BRÜGGEMANN*
Institut für Physik, Carl von Ossietzky Universität Oldenburg, 26111 Oldenburg, Germany

As the photovoltaic efficiency of heterojunction solar cells based on amorphous and crystalline silicon depends critically on the quality of the front and rear interfaces, characterisation techniques for intermediate steps during processing are helpful in the optimisation of these devices. Photoluminescence techniques allow the probing of the minority carrier density, which sensitively depends on the interface properties. We present modulated photoluminescence as a technique to characterise the interface quality by the determination of the excess carrier lifetime. We apply numerical simulation to illustrate various aspects of the detrimental influence of the interface defects on the photovoltaic properties and the electroluminescence yield of these devices. The simulation indicates that optimised interfaces of these heterojunction solar cells lead to high photovoltaic conversion efficiencies in excess of 23% and high electroluminescence efficiencies of 0.14%.

(Received November 5, 2008; accepted December 15, 2008)

Keywords: Solar cells, Photoluminescence, Electroluminescence, Efficiency, Interfaces

1. Introduction

Heterojunction silicon solar cells have reached photovoltaic efficiencies in excess of 22% [1]. The structure of these cells is sketched in Fig. 1. It consists of a monocrystalline silicon (c-Si) wafer with thin layers of doped and undoped hydrogenated amorphous silicon (a-Si:H) to form the junction. In the Sanyo HIT solar cell [1], an intrinsic thin layer is deposited between the wafer and the doped amorphous layer (Fig. 1, right). The so-called back-surface field (BSF) layers of a-Si:H are not shown in the figure. While the Sanyo concept is based on n-type c-Si wafers, Fig. 1 indicates that it is in principal possible to construct these kinds of solar cells with p-type c-Si. The base material may also be multicrystalline or low-cost silicon.

For many years, and still as ongoing research, the optimisation of these structures has concentrated on the properties of the interface between the front a-Si:H layers and the c-Si wafer, for which both the wafer pre-treatment prior to the amorphous silicon deposition and the a-Si:H deposition itself, typically by plasma enhanced chemical vapour deposition (PECVD), are important, e.g. [1-5]. In addition, the back-contact properties have been investigated and improved.

Because of the detrimental effect of the interface defects on the device properties, characterisation techniques are required not only for the fully processed cells but for the wafer structures with various deposited amorphous silicon layers. Recent research activities have in common that the characterisation of the passivated wafers has contributed to the solar cell optimisation: In Europe, national network projects were established. A summary of the results of the German project on both n and p type wafers can be found in [2]. In the French network [3] alternative thin layers of polymorphous silicon have been deposited to optimise the heterojunction cells, also in view of industrial processes. The focus of the heterojunction research at National Renewable Energy Laboratory (NREL) [4] is on alternative deposition techniques like hot-wire chemical vapour deposition for the amorphous layers. In Neuchatel, very-high frequency PECVD has been applied to process heterojunction solar cells with high open-circuit voltages [5].

The consequent application by the quasi-steady state photoconductance, microwave-detected photocarrier decay or photoluminescence technique has lead to better interface properties and higher open-circuit voltages. Typically, one may optimise the passivated wafers (for example with respect to the pre-treatment of the wafer prior to the a-Si:H deposition, doping, pressure, deposition temperature, i-layer / no i-layer) and transfer the expertise to the deposition and processing of the solar cells.

In order to assist in the understanding of the device physics and optimisation, device simulation gives an insight into the device properties. For this reason, simulation programmes have been developed, namely SC-Simul [6,7] and AFORS-HET [8,9] with particular emphasis on the simulation of Si heterojunction solar cells. For example, the influence of interface defects on the device in the dark and under illumination can be studied. Based on the numerical results, it was shown [10] that the a-Si:H/c-Si heterostructure based on n-type wafers with holes as minority carriers is less affected by the interface defects than p-type wafer structures, because of the reduced minority-carrier related interface-recombination rate in the former.

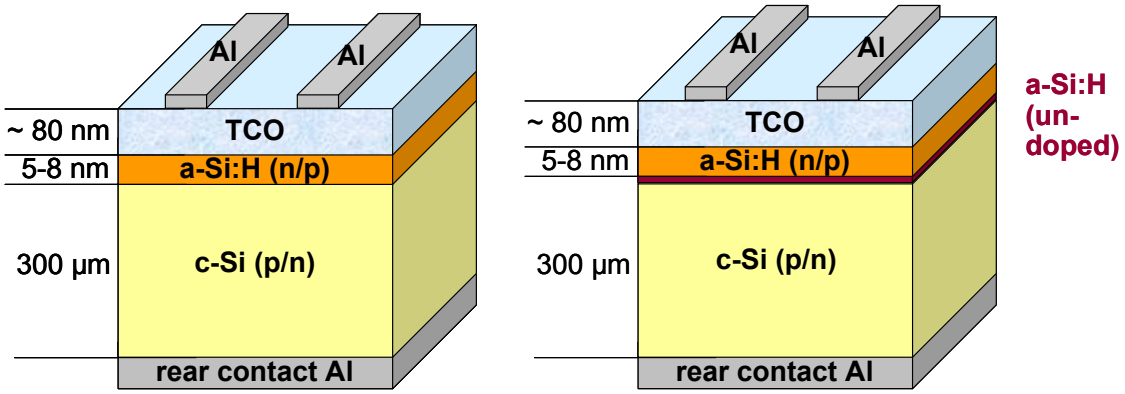

Fig. 1. Sketch of typical heterojunction silicon solar cells with either p-type c-Si / n-type a-Si:H or n-type c-Si / p-type a-Si:H. The right hand cell has an additional thin undoped a-Si:H layer, thought to improve the interface properties. Highly doped amorphous layers may also serve as so-called back-surface field layers, not included in the sketch..

In the present work, we present the application of photoluminescence techniques for interface characterisation. We also apply numerical modelling to give further insight as to how the interface defects influence the solar cell device properties. Significant possible achievements can be deduced from the numerical modelling results with optimised solar cells, with respect to the photovoltaic properties and also in terms of a high electroluminescence efficiency of these c-Si diodes.

2. Experimental techniques

The photoluminescence techniques are based on collecting luminescence radiation from the bulk of the c-Si wafer, which may either be measured integratively, i.e., photons of the whole spectrum are collected by a suitable photodiode, or spectrally dispersed by a monochromator or spectrograph with suitable detection equipment.

For modulated photoluminescence (MPL), the photogeneration rate is described by [11]

$$G = G_0 + G_1 \, e^{i\omega t} \tag{1}$$

so that in the steady state with $G = G_0 = \Delta n_0 / \tau_n$, a lifetime τ_n can be defined. With the Ansatz

$$\Delta n = \Delta n_0 + \Delta n_1 \, e^{i\omega t} \tag{2}$$

for the excess minority carrier density Δn in a p-type wafer, Δn_1 is complex with the amplitude

$$|\Delta n_1| = \frac{\tau_n G_1}{\left(1+\omega^2 \tau_n^2\right)^{1/2}} \tag{3}$$

and with the phase Φ with respect to G_1

$$\tan \Phi = -\omega \tau_n. \tag{4}$$

This simple model assumes that the combination of the bulk lifetime and the surface recombination velocity S results in a homogeneous carrier distribution and an effective lifetime τ_n of the minority carriers.

Fig. 2 shows the spatial profile of the minority carrier density for steady-state illumination [12]. The minority-carrier densities remain spatially constant for a symmetrical wafer structure with equal front (S_0) and rear (S_r) surface recombination velocities < 1000 cm/s and a bulk lifetime of a few hundred µs.

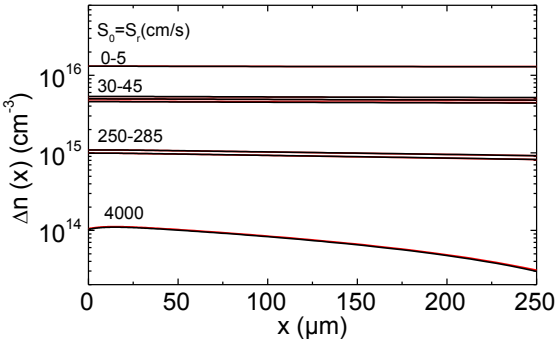

Fig. 2. Excess carrier densities of a c-Si wafer for the variation of the surface recombination velocities S_0 and S_r at the front and the rear. The illumination is from the left and for a bulk lifetime of about 700 µs (after [12]).

For very short lifetimes and/or high surface recombination velocities, the assumption of a homogeneous carrier distribution does not hold any longer. In that case a more detailed analysis is required, as outlined in [13] in the work on modulated photocarrier radiometry.

For the spectrally resolved luminescence of band-to-band recombination, the emitted photon flux density into one hemisphere of a symmetrical wafer structure can be described by the quasi-Fermi levels of the conduction-band electrons and the valence-band holes, ε_{Fn} and ε_{Fp} [14]

$$\mathrm{d}j_\gamma(\hbar\omega) = \frac{(\hbar\omega)^2}{4\pi^2\hbar^3 c^2} \times A(\hbar\omega) \exp\left(\frac{\hbar\omega}{kT}\right) \exp\left(\frac{\varepsilon_{Fn} - \varepsilon_{Fp}}{kT}\right) \mathrm{d}\hbar\omega \quad (5)$$

where A is the absorptivity of the sample, which reads for a symmetrical wafer as

$$A(\hbar\omega) = \frac{(1 - R_{int}(\hbar\omega))(1 - e^{-\alpha(\hbar\omega) d})}{1 - R_{int}(\hbar\omega)}. \quad (6)$$

Here, R_{int} is the reflection coefficient of the air/wafer interface, d is the sample thickness and α is the absorption coefficient.

In Eq. (5), the assumption has been made that ε_{Fn} - ε_{Fp} is spatially constant. The spectral shape of the emitted radiation is thus mainly determined by the product of the energy-dependent Boltzmann term and the absorptivity of the sample structure under study. The height of the spectrum is scaled by the exponential dependence on $\varepsilon_{Fn} - \varepsilon_{Fp}$, which reflects the product of the free electron and hole densities, together with the kT term.

For non-homogeneous carrier distributions and a non-constant quasi-Fermi level splitting, a more complicated version of Eq. (5) involves an integral term to take into account the non-homogeneous generation and propagation of the luminescence photons [15]. In addition, the term for A is modified, for example in a solar cell with a rear-side mirror-like contact.

The emitted electroluminescence radiation of a solar cell depends on the applied voltage V_a. Würfel [14] pointed out that for a good luminescent p-n diode, with the quasi-Fermi level splitting being almost constant in space, $\varepsilon_{Fn} - \varepsilon_{Fp}$ in the whole volume equals eV_a, and thus from Eq. (5) it follows that

$$\mathrm{d}j_\gamma(\hbar\omega) = \frac{(\hbar\omega)^2}{4\pi^2\hbar^3 c^2} \times A(\hbar\omega) \exp\left(\frac{\hbar\omega}{kT}\right) \exp\left(\frac{eV_a}{kT}\right) \mathrm{d}\hbar\omega \quad (7)$$

3. Simulation

The simulation software SC-Simul [6,7] allows the device modelling of heterojunction solar cells with different layers which can be modified individually to build a device. The programme allows one to determine all the physical properties of interest, e.g., the quasi-Fermi levels or the free electron and hole densities, the electrostatic potential and other properties like recombination rates. The input parameters are the semiconductor properties of the different layers with which a structure is built, like the band gap E_g, effective densities of states in the band, free carrier mobilities, electron affinity, capture coefficients for defect states and parameters for defect densities and distributions.

4. Results and discussion

4.1. Modulated photoluminescence

The MPL technique has been applied in [11] for the characterisation of the effective minority carrier lifetimes in a variety of passivated c-Si wafers. The MPL lifetime, which corresponds well to the decay time of the PL signal after the termination of the illumination, thus gives valuable information on the quality of the interface between the c-Si wafer and the passivation layers. More recently, it was shown that the MPL lifetimes in the wafers correspond to lifetimes determined by the quasi-steady state photoconductance technique [16] – as long as the lifetime is long enough to ensure a homogeneous carrier profile. The study of a sample sequence of wafers, measured with MPL, and further processed cells, measured by a low-frequency capacitance technique [17], showed a good correlation between the results from wafers and cells [18].

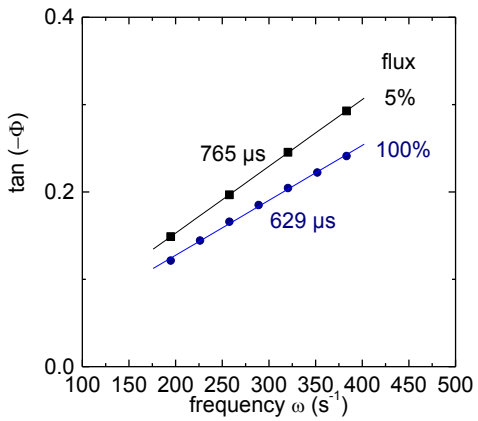

Fig. 3. The frequency-dependent room-temperature MPL signal of a double- heterojunction wafer structure. The corresponding solar cells reached open-circuit voltages of around 700 mV. The effective lifetimes for the two photon fluxes are indicated. The 100% flux corresponds to 3 × 10^{18} cm^{-2} s^{-1} at 655 nm.

Fig. 3 documents the long effective lifetimes that have been achieved at the University of Neuchatel after systematic characterisation by the quasi-steady state photoconductance technique with deposition-parameter optimisation of passivated wafers [5,19].

The figure illustrates the measured linear variation of the tangent of the MPL phase shift with modulation frequency of such a double-heterojunction structure from Univ. Neuchatel. The long effective lifetimes, determined from the slope, indicate that the interfaces are well passivated. Effective lifetime measurements by the quasi-

steady state photoconductance technique on comparable structures show similar high values [19]. The systematic characterisation of the interface properties of passivated wafers has been the major instrument in optimising the solar cells themselves. Olibet et al. [19] reported open-circuit voltages around 700 mV via such an optimisation strategy.

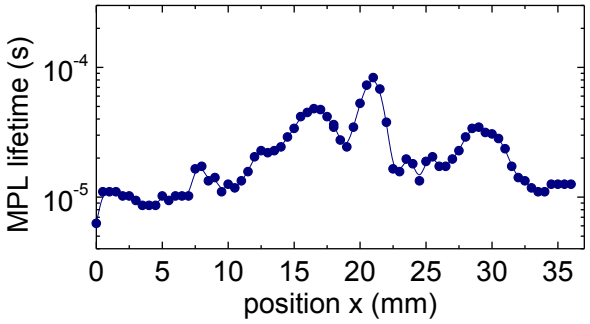

Fig. 4. MPL lifetime vs. position of a passivated multicrystalline Si wafer.

Fig. 4 shows that the MPL technique can also be applied to scan different regions of a passivated wafer. The specimen is a silicon-nitride passivated multicrystalline silicon wafer. Here, after checking the linear variation of tan(Φ) with modulation frequency (Eq. (4)), the scan was performed by determination of the lifetime from a single-frequency measurement only. This procedure results in a faster scan speed than the evaluation of the slopes.

The spatial variations in the MPL-derived lifetime correspond well to the lifetimes determined from the microwave-detected photocarrier decay [20].

As the phase is measured in the MPL experiment, the results are less affected by variations in the photogeneration rate, for example by different spatially dependent reflection properties, which would directly change the PL amplitude.

As mentioned above, the analysis of the MPL phase depends on a simple model. From the point of view that we deal with the characterisation of samples that have minority carrier properties suitable for solar cell applications, this may be sufficient. Leong et al. [21] applied their photocarrier radiometry analysis on a-Si:H passivated c-Si wafers with low effective lifetimes. In such a case their analysis is more thorough, but the MPL analysis would still give a fingerprint of the samples because of the low detected phase shift. A qualitative conclusion can thus be made that relates poor interface properties to not being able to measure significant phase shifts.

A number of reports have linked the photoluminescence yield from spectrally resolved measurements with the interface properties. The change in the PL yield for different processing steps provided information on favourable deposition parameters or the influence of the contact preparation, for which the reader is referred to [2,22].

Table 1. Summary of the simulated solar cell properties.

	N_{if} (10^{10} cm^{-2})	S_r (cm/s)	$\eta_{AM1.5}$ (%)	V_{oc} (mV)	j_0 (fA cm^{-2})
A	2	1	23.64	718.3	57.2
B	2	100	23.15	702.2	79.4
C	200	1	20.64	630.0	1449.2

4.2. Simulation of interface-related properties

The above-mentioned influence of the interface quality on the photovoltaic properties of heterojunction solar cells can be studied in detail by numerical simulation. Fig. 5 shows the currents in the dark and under illumination of a 300 µm thick (n)a-Si:H/(p)c-Si solar cell with rear-surface recombination velocities of the minority carriers S_r of 1 cm/s and 100 cm/s. Relevant parameters and results of Fig. 5 are summarised in Table 1.

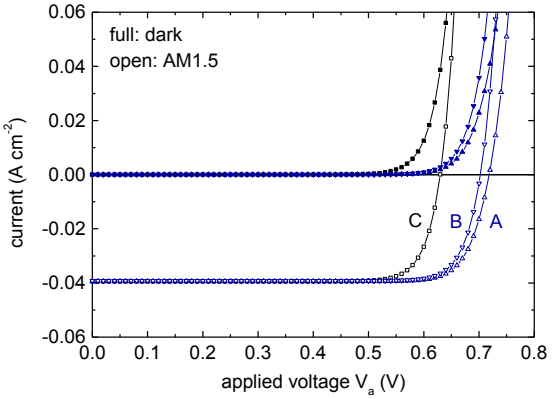

Fig. 5. Current-voltage characteristics in the dark and under AM1.5 illumination of three heterojunction solar cells A, B and C, with different interface defect densities or back contact properties, see Table 1.

The comparison of cells A and C with the same S_r shows that the front a-Si:H/c-Si interface determines the current properties for these two cells, with interface densities N_{if} of 2×10^{10} cm^{-2} and 2×10^{12} cm^{-2}. The change in the voltage-dependent total current under illumination for the higher N_{if} almost follows the change in the dark current density. There is a significant increase in the dark current saturation current density j_0 with increases in N_{if}.

With the higher interface defect density, the photovoltaic conversion efficiency $\eta_{AM1.5}$ of cell C under AM1.5 illumination is 20.64%, compared to 23.64% of cell A with the lower N_{if}. There is an additional loss of photogenerated carriers, as the fill-factor is slightly lower for cell C. The results for cell B in Fig. 5 indicate that an increase in S_r to 100 cm/s results in an increase in j_0 compared to the case of cell A, and in a slight decrease in V_{oc} and $\eta_{AM1.5}$. Further increase of S_r results in lower values of V_{oc}, as indicated in Fig. 6 where V_{oc} saturates at slightly above 0.64 V.

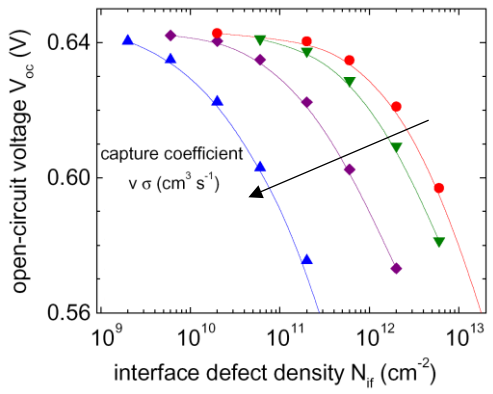

Fig. 6. Variation of the open-circuit voltage with interface defect density with the capture coefficient as an additional parameter.

Fig. 6 illustrates the variation in V_{oc} with increasing N_{if} for cells with an Ohmic back contact. An increase in the capture coefficients also leads to an enhanced drop in the open-circuit voltage. It confirms that the interface defect density is not the only parameter that influences the drop in V_{oc}. It is thus not possible to deduce the value of N_{if} without further information.

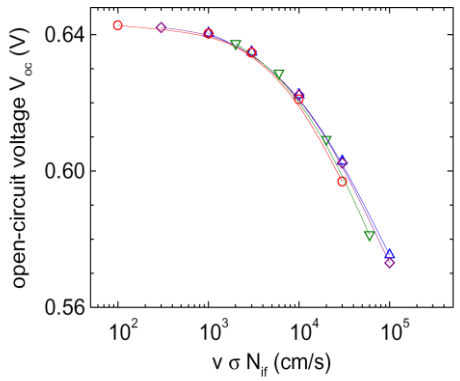

Fig. 7. The data of Fig. 6, re-plotted, to show the influence of the effective surface recombination velocity on the open-circuit voltage. One set of symbols represents one value of the capture coefficient.

Fig. 7 shows V_{oc} vs. the product of the capture coefficient νσ (the product of thermal velocity and capture cross-section) and interface density N_{if}. Its units are that of a velocity and, within the range depicted in Fig. 7, $\nu\sigma N_{if}$ can indeed be regarded as a surface recombination velocity. Because of the Ohmic back contact, the front effective surface recombination velocity can be as high as 1000 cm/s before it induces a further drop in V_{oc}. At higher interface-defect densities, the charge character of these states leads to some spreading of the V_{oc} data for poor devices.

Fig. 8 illustrates the role of the dangling-bond defects in the (n)a-Si:H layer, which were varied together with the interface defect density and also with the quality of the rear contact. The diffusion lengths in the c-Si were greater than the cell thickness. A BSF layer was introduced, which results in V_{oc} close to 710 mV.

The defect density in the doped a-Si:H layer does not influence V_{oc}. Once minority carriers have reached the junction and entered the layer with its opposite doping, they recombine no matter what the dangling-bond density is.

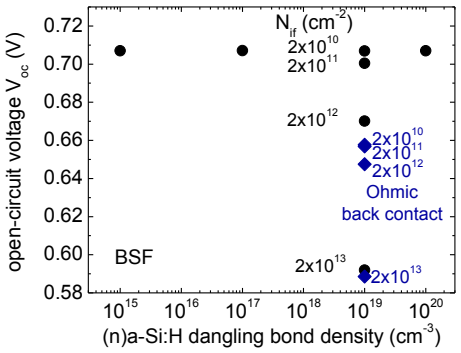

Fig. 8. Variation of the open-circuit voltage for a changing dangling-bond density in the doped amorphous layer with a BSF (circles). The influence of an Ohmic contact is also shown (diamonds).

For the BSF case, the front a-Si:H/c-Si interface defect density N_{if} remains the limiting parameter. This case is depicted by the vertical set of data points (circles) at a 10^{19} cm^{-3} dangling bond density. Generally, it can be seen that with the Ohmic back contact, the V_{oc} values are much lower – apart for the highest N_{if} values when the front interface dominates the whole device whatever the back contact is.

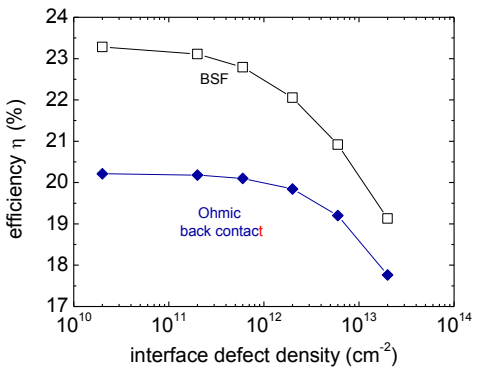

Fig. 9. The efficiency $\eta_{AM1.5}$ of the solar cells of Fig. 8, showing the limitation imposed by a poor back contact on the photovoltaic efficiency

Fig. 9 illustrates again that AM1.5 conversion efficiencies $\eta_{AM1.5}$ in excess of 23% can be reached in the simulation.

4.3. Electroluminescence

The density of interface defects also influences the photoluminescence and electroluminescence yield of the heterojunction solar cells [7-9,22-24]. Fig. 10 illustrates the variation in the spatially integrated band-to-band recombination rate or relative electroluminescence yield for the three cells in Table 1 and Fig. 5. Similar to the photovoltaic properties, cell C shows the poorest performance with its higher N_{if}.

At the same current density, the lower rear surface recombination velocity leads to some higher band-to-band recombination rate in cell A than in cell B.

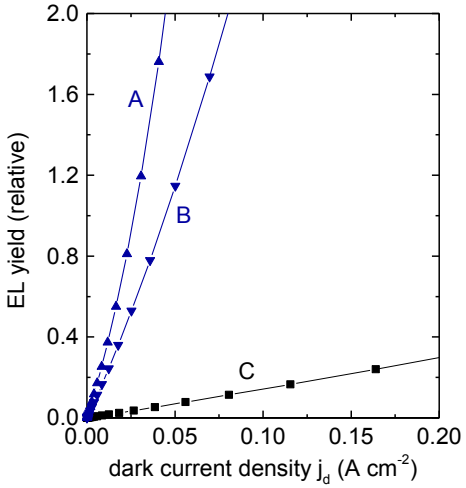

Fig. 10. The spatially integrated band-to-band recombination rate as a measure of the EL yield for the solar cells A, B and C.

Fig. 11 displays the simulated EL emission spectra of the three cells at an applied voltage of 652 mV. The spatial variation of the quasi-Fermi energies was determined by SC-Simul, and a modified version of Eq. (7) (given for example in [15]) was applied to calculate the spectra. In this expression, the spatial variation of the carrier densities and the reflectivities of the contacts in the absorptivity A ($\hbar$ is taken into account.

The symbols, representing the data points in Fig. 11, are very close for the different cells, which indicates that the carrier densities are almost homogenous. The diffusion length is greater than the device thickness, and the chosen values of N_{if} and S_r do not modify the spatial distributions. This is confirmed by inspection of the carrier distributions from SC-Simul. Indeed, the application of Eq. (7) results in the same spectrum as in Fig. 11.

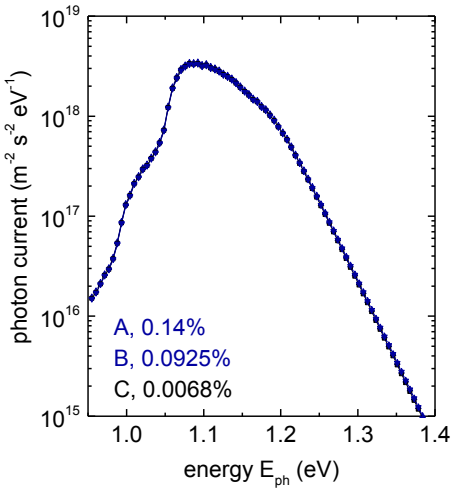

Fig. 11. Electroluminescence spectra of the cells A, B, and C, in terms of the emitted photon current density into one hemisphere at V_a = 652 mV. The efficiency η_{ext} is also given.

The dark current densities that drive the electroluminescence processes are very much different for cell C compared with A and B. For the higher interface defect densities, a higher current is needed to maintain the quasi-Fermi level splitting that corresponds to the applied voltage.

Integration of the spectra gives an emitted photon-current density J_{ph} into one hemisphere. With the particle-current density, determined by $J_{el} = j_{el}/e$, where j_{el} is the electrical current density measurable in the external electrical circuit, and e is the electron charge, an external radiative efficiency can be defined by $\eta_{ext} = J_{ph}/J_{el}$. Fig. 11 also details the values of η_{ext}.

The simulated efficiency of 0.14% shows the potential of the heterostructures to be efficient radiation emitters if a low interface defect density and thus a high open-circuit voltage, which in turn corresponds to a low saturation-current density, can be achieved. The link between V_{oc} and the EL efficiency has been made in [25]. Power efficiencies of around 0.03% have been reported on a-Si/c-Si solar cells with open-circuit voltages below 640 mV [25,26]. Recent measurements on solar cells with V_{oc} in excess of 700 mV indicate that electroluminescence efficiencies higher than 0.03% can indeed be achieved experimentally [27].

5. Conclusions

We have presented variations of photoluminescence techniques to characterise heterostructures of amorphous and crystalline silicon. From the MPL experiment, effective lifetimes can be deduced, and the quality of the interfaces can be evaluated. Such a characterisation is helpful for the optimisation of the interface properties and back-contact effects, and the expertise gained can be transferred to the device preparation. The simulation results for solar cells have shown that the interface defects

mainly affect V_{oc}. For the simulated high photovoltaic conversion efficiency in the range of 23% of these heterojunction solar cells, it is also necessary to have a high quality back contact. A simulated EL efficiency of 0.14% has been demonstrated for a heterojunction solar cell with an open-circuit voltage of 718 mV.

Acknowledgments

The author thanks S. Olibet from the University of Neuchatel and colleagues at ISFH for providing samples. The author is also grateful to colleagues at Oldenburg University and LGEP for collaboration.

References

[1] Y. Tsunomura M. Taguchia, T. Babaa, T. Kinoshitaa, H. Kannoa, H. Sakataa, E. Maruyamaa, M. Tanaka, Solar En. Mat. Solar Cells (2008), doi:10.1016/j.solmat.2008.02. 037, in press.

[2] K. v. Maydell, H. Windgassen, W. A. Nositschka, U. Rau, P. J. Rostan, J. Henze, J. Schmidt, M. Scherff, W. Fahrner, D. Borchert, S. Tardon, R. Brüggemann, H. Stiebig, M. Schmidt European Photovoltaic Solar Energy Conference, September 2005, Barcelona, Spain, eds.: W. Palz, H. Ossenbrink , P. Helm (WIP, Munich 2005) p. 822.

[3] P.-J. Ribeyron, A. Vandeneynde, J. Damon-Lacoste, D. Eon, P. Roca i Cabarrocas, R. Chouffot, J.-P. Kleider, R. Brüggemann, Proc. 22nd European Photovoltaic Solar Energy Conference, September 2007, Milan, Italy, (WIP, Munich, 2007) p. 1197.

[4] H. M. Branz, C. W. Teplin, D. L. Young, M. R. Page, E. Iwaniczko, L. Roybal, R. Bauer, A. H. Mahan, Y. Xu, P. Stradins, T. Wang, Q. Wang, Thin Solid Films **516**, 743 (2008).

[5] S. Olibet, E. Vallat-Sauvain, C. Ballif, L. Korte, L. Fesquet, Proceedings of the 17th Workshop on Crystalline Silicon Solar Cells and Modules: Materials and Processes, Vail, Colorado USA, August, 2007, p. 130.

[6] M. Rösch, PhD Thesis (in German), available online at http://docserver.bis.uni-oldenburg.de/publikationen/dissertation/2003/roeexp03/roeexp03.html

[7] R. Brüggemann, M. Rösch, J. Optoelectron. Adv. Mater. **7**, 65 (2005).

[8] A. Froitzheim, R. Stangl, M. Kriegel, L. Elstner, W. Fuhs, Proc. 3rd World Conference on Photovoltaic Energy Conversion, Osaka, Japan, May 2003, eds. K. Kurokawa, L.L. Kazmerski, B. McNelis, M. Yamaguchi, C. Wronski, W.C. Sinke (Osaka, 2003), p. 279.

[9] R. Stangl, A. Froitzheim, M. Kriegel, T. Brammer, S. Kirste, L. Elstner, H. Stiebig, M. Schmidt, W. Fuhs, Proc. 19th European Photovoltaic Solar Energy Conference, Paris, France, June 2004, p. 1497.

[10] M. Rösch, R. Brüggemann, G. H. Bauer, 2nd World Conference on Photovoltaic Solar Energy Conversion, Vienna, Eds. J. Schmid Schmid J, H.A. Ossenbrink, P. Helm, H. Ehmann, E.D. Dunlop, Joint Research Centre, Ispra, 1998, p. 946.

[11] R. Brüggemann, S. Reynolds, J. Non-Cryst. Solids **352**, 1888 (2006).

[12] S. Tardon, PhD Thesis, Universität Oldenburg (2006).

[13] A. Mandelis, J. Batista, D. Shaughnessy, Phys. Rev. B **67**, 205208 (2003).

[14] P. Würfel, J. Phys. C **15**, 3967 (1982).

[15] T. Trupke, E. Daub, P. Würfel, Solar Energy Materials Solar Cells **53**, 103 (1998).

[16] R. Chouffot, A. Brezard-Oudot, J.-P. Kleider, R. Brüggemann, M. Labrune, P. Roca i Cabarrocas, P.-J. Ribeyron, accepted in Mat. Science and Engineering B.

[17] A. S. Gudovskikh, R. Chouffot, J. P. Kleider, N. A. Kaluzhniy, V. M. Lantratov, S. A. Mintairov, J. Damon-Lacoste, D. Eon, P. Roca i Cabarrocas, P.-J. Ribeyron, Thin Solid Films, **516**, 6786 (2008).

[18] R. Chouffot, S. Ibrahim, R. Brüggemann, A. S. Gudovskikh, J. P. Kleider, M. Scherff, W. R. Fahrner, P. Roca i Cabarrocas, D. Eon and P.-J. Ribeyron, J. Non-Cryst. Solids **354**, 2416 (2008).

[19] S. Olibet, E. Vallat-Sauvain, C. Ballif, L. Fesquet, Proc. NUMOS-workshop (Numerical modelling of thin film solar cells), Gent, Belgium, March, 2007, p. 141.

[20] R. Brüggemann, G. H. Bauer, BMBF project report (available from the author).

[21] K. R. Leong, A. Mandelis, N. P. Kherani, S. Zukotynski, in Amorphous and Polycrystalline Thin-Film Silicon Science and Technology — 2006, eds.: S. Wagner, V. Chu, H. A. Atwater, Jr., K. Yamamoto, H.-W. Zan (MRS Symp. Proc. 910, Warrendale, PA, 2007), A06-03.

[22] S. Tardon, M. Rösch, R. Brüggemann, T. Unold, G. H. Bauer, J. Non-Cryst. Solids **338**, 444 (2000).

[23] G. H. Bauer, R. Brüggemann, M. Rösch, S. Tardon, T. Unold, Phys. Status Solidi (c) **1**, 1308 (2004).

[24] R. Brüggemann, M. Rösch, S. Tardon, G. H. Bauer, in Amorphous and Nanocrystalline Silicon Science and Technology—2005, eds.: R. W. Collins, P. C. Taylor, M. Kondo, R. Carius, R. Biswas (MRS Symp. Proc. 862, Warrendale, PA, 2005), A9.3.

[25] W. Fuhs, A. Laades, K. von Maydell, O.B. Gusev, E. Terukov, S. Kazitsyna-Baranovski, G. Weiser, J. Non-Cryst. Solids **352**, 1884 (2006).

[26] G. Weiser, private communication, the correct power-efficiency value is 0.032% instead of the 0.32% of [25].

[27] R. Brüggemann, to be published.

*Corresponding author: rudi.brueggemann@uni-oldenburg.de